Overcoming Intrinsic Material Limitations through Cavity Feedback

M. Ebrahimi,[1] Y. Huang,[1] V. A. S. V. Bittencourt,[2] A. Rashedi,[1] A. Metelmann,[2,3] and J. P. Davis[1,*]

[1]*Department of Physics, University of Alberta, Edmonton, Alberta T6G 2E9, Canada*

[2]*Institut de Science et d'Ingénierie Supramoléculaires (ISIS, UMR7006), Université de Strasbourg, 67000 Strasbourg, France*

[3]*Institute for Theory of Condensed Matter and Institute for Quantum Materials and Technology, Karlsruhe Institute of Technology, 76131, Karlsruhe, Germany*

(Received 11 March 2026; accepted 13 August 2026; published 14 September 2026)

Magnons, the quanta of spin waves, have significant potential for use in modern technologies, especially when they are strongly coupled to another mode for readout and control. Although magnons strongly interact with microwave photons via the magnetic-dipole interaction to form hybrid cavity-magnon polariton modes, the magnon-phonon interaction in micrometer-sized ferromagnetic spheres is typically weak, which is further aggravated by the large polariton linewidths dominated by the magnon dissipation. The material-limited magnon dissipation rate in particular has been regarded as an unavoidable limitation in these systems. Here, we surpass this long-standing limitation by implementing an active microwave feedback loop to suppress the linewidth of cavity-magnon polaritons and reduce their effective decay rate below the magnon-limited linewidth, thereby enhancing the polariton-phonon cooperativity from $C \simeq 1$ to $C \simeq 300$. As a key milestone, we achieved normal-mode splitting between a cavity-magnon polariton and a mechanical mode, providing direct evidence of three-mode hybridization among photons, magnons, and phonons. Our results establish feedback as a general route to accessing strong-coupling regimes in systems previously thought to be limited by material properties and hence open new opportunities for coherent control in hybrid quantum systems.

DOI: 10.1103/pbbp-bz28

Subject Areas: Condensed Matter Physics, Magnetism, Mechanics

I. INTRODUCTION

The premise of hybrid quantum systems is to use the best properties of individual subsystems to create new complementary functionalities [1]. For example, magnons offer the possibility of new magnetic sensing paradigms [2,3], or nonreciprocity, enabling new circulators and isolators [4–6] or nonreciprocal wavelength transducers [7]. When introduced into a microwave cavity, magnons interact strongly with cavity photons forming cavity polaritons [8–14], deemed cavity magnonics. Magnons and MHz-frequency phonons, e.g., from elastic breathing modes of sub-mm spheres [15,16], couple via a radiation-pressure-like interaction: elastic vibrations modulate the magnon resonance frequency, and the magnetization precession causes elastic deformations. This effect forms the basis of cavity magnomechanics, leading to the magnetostrictive version of dynamical backaction effects [15,16]. A distinctive feature of cavity magnomechanics is the triple-resonance condition, in which the phonon frequency matches the frequency difference between the hybrid cavity-magnon polariton modes, enabling selective enhancement of magnon-phonon scattering processes [15,16]. This regime has attracted significant interest and motivated proposals for a wide range of applications, including the generation of nonclassical entangled states [17–22], squeezed states [23], classical and quantum information processing [24–26], quantum correlation thermometry [27], quantum nondemolition measurement [28], and the exploitation of parity-time (PT) symmetry [21,29].

Despite these appealing features, cavity magnomechanics has so far remained firmly in the weak-coupling regime. While the photon-magnon interaction can readily reach the strong-coupling regime, the parametric magnetostrictive magnon-phonon interaction is weak in sub-mm spheres, where the photon-magnon interaction is the strongest. More importantly, the linewidth of the hybrid cavity-magnon polariton is dominated by intrinsic magnon dissipation arising from material properties, since the microwave photon dissipation rate can be tailored by engineering the microwave cavity [30–32]. Such material-limited dissipation rates cannot be overcome by increasing the drive strength alone and therefore have been

[*]Contact author: jdavis@ualberta.ca

widely regarded as an unavoidable barrier preventing access to the strong magnomechanical coupling regime. As a result, although hybrid cavity-magnon interactions have been studied both theoretically [13,14,33–37] and experimentally [12,38–49], experimental investigations of magnomechanical coupling have remained limited, with all studies confined to the weak-coupling regime [15,16,50].

Feedback provides a powerful framework for controlling hybrid quantum systems by actively modifying their dynamical properties [51–60]. In conventional feedback schemes, measurement outcomes are processed and fed back to the system to engineer their effective response. In cavity optomechanical systems, one widely used approach is to feed the cavity output field back to the mechanical oscillator, thereby providing force actuation that enables efficient cooling of the mechanical motion [53,57,60]. Such mechanical feedback has proven highly successful, particularly for enhancing cooling performance in the unresolved-sideband regime. An alternative feedback configuration feeds the cavity output field back to the cavity mode itself [51,52]. In this case, the feedback modifies the effective cavity susceptibility, which, in turn, alters the optomechanical response in the strong-coupling regime. However, applying feedback to the cavity mode does not provide a similarly stunning advantage in enhancing the optomechanical cooperativity. This is because the optomechanical interaction is fundamentally parametric, and the linearized coupling strength can be increased simply by increasing the intracavity drive power. Consequently, comparable enhancements of the optomechanical cooperativity can generally be achieved without cavity feedback by employing stronger drive tones [61,62]. This situation is fundamentally different in cavity magnomechanical systems, where the intrinsic magnon dissipation constitutes a material limitation that cannot be overcome by increasing the drive power alone because of the resonant nature of the photon-magnon interaction. Here, we demonstrate both theoretically and experimentally that applying feedback to the cavity mode overcomes this limitation, providing a clear and unique advantage for cavity magnomechanical systems.

We experimentally implement an active microwave feedback loop to engineer the dissipation of cavity-magnon polaritons. By feeding the cavity output back into the system with tunable gain and phase, we suppress the effective polariton decay rate by more than an order of magnitude, reducing it below the intrinsic magnon dissipation rate and thereby overcoming a fundamental limitation of the system. As a result, the magnomechanical cooperativity, which is inversely proportional to the polariton dissipation rate, increases from $C \simeq 1$ to $C \simeq 300$, enabling the magnomechanical coupling rate to exceed the total dissipation rate and leading to the observation of normal-mode splitting between a mechanical mode and a cavity-magnon polariton. The resulting high magnomechanical cooperativity constitutes a key prerequisite for further studies of coherent energy exchange [52,61,62], ground-state mechanical cooling [51,63–65], and transduction between magnonic, mechanical, and microwave degrees of freedom [7]. These results demonstrate that microwave feedback provides a general route to overcoming material-limited dissipation, enabling access to strong-coupling regimes that were previously unattainable. Our results establish a deterministic three-mode hybrid system and represent a starting point for future experimental studies in cavity magnomechanics, especially those reaching into the quantum regime [12,17–22,25,66–70].

II. EXPERIMENTAL SETUP AND FEEDBACK-ENABLED OVERCOMING INTRINSIC MAGNON DISSIPATION

Our experiment employs a three-dimensional copper microwave cavity, allowing application of bias magnetic fields, with inner volume $30 \times 30 \times 2.5\ \mathrm{mm}^3$, operated at room temperature and supporting a fundamental TE_{101} mode [16] at $\omega_a/2\pi \approx 7.1338$ GHz. The cavity is coupled to two external ports, enabling independent access for weak probing, coherent pump tones, and the implementation of an active microwave feedback loop. The intrinsic cavity decay rate is $\kappa_{\mathrm{int}}/2\pi \approx 3.18$ MHz, while the total external coupling rate, with both ports connected, is $\kappa_{\mathrm{ext}}/2\pi = (\kappa_{\mathrm{ext}}^{(1)} + \kappa_{\mathrm{ext}}^{(2)})/2\pi \approx 1.24$ MHz.

A single-crystal yttrium iron garnet (YIG) sphere with a radius of 200 μm and an intrinsic magnon dissipation rate $\kappa_m/2\pi = 2.20$ MHz is positioned near the magnetic-field antinode of the cavity mode yielding the magnon-microwave coupling rate $g_{ma}/2\pi = 5.84$ MHz. The orientation of the sphere is fixed by a static magnetic field applied along its easy axis. This field is generated by a pair of permanent magnets, as shown schematically in Fig. 1(a), and can be finely tuned using a 104-turn solenoid wound around a pure iron core and coupled via an iron yoke [71]. The bias magnetic field enables precise tuning of the uniform magnon mode frequency $\omega_m = \gamma B_0$, where $\gamma = 28$ GHz/T and B_0 is the bias field, thereby allowing control of the cavity-magnon polariton modes, as shown in Fig. 1(b).

To investigate feedback-induced modifications of the cavity-magnon polariton modes in the absence of mechanical excitation, the cavity is first probed through port 1 using a weak microwave signal. The output field from port 2 is divided using a power splitter: one arm is directed to a vector network analyzer (VNA) for transmission measurements, while the other arm is routed through a phase shifter and tunable-gain microwave amplifier before being fed back into the cavity through port 1 via a directional coupler, as illustrated in Fig. 1(a).

In the absence of feedback, the microwave cavity-magnon system is governed by the standard microwave

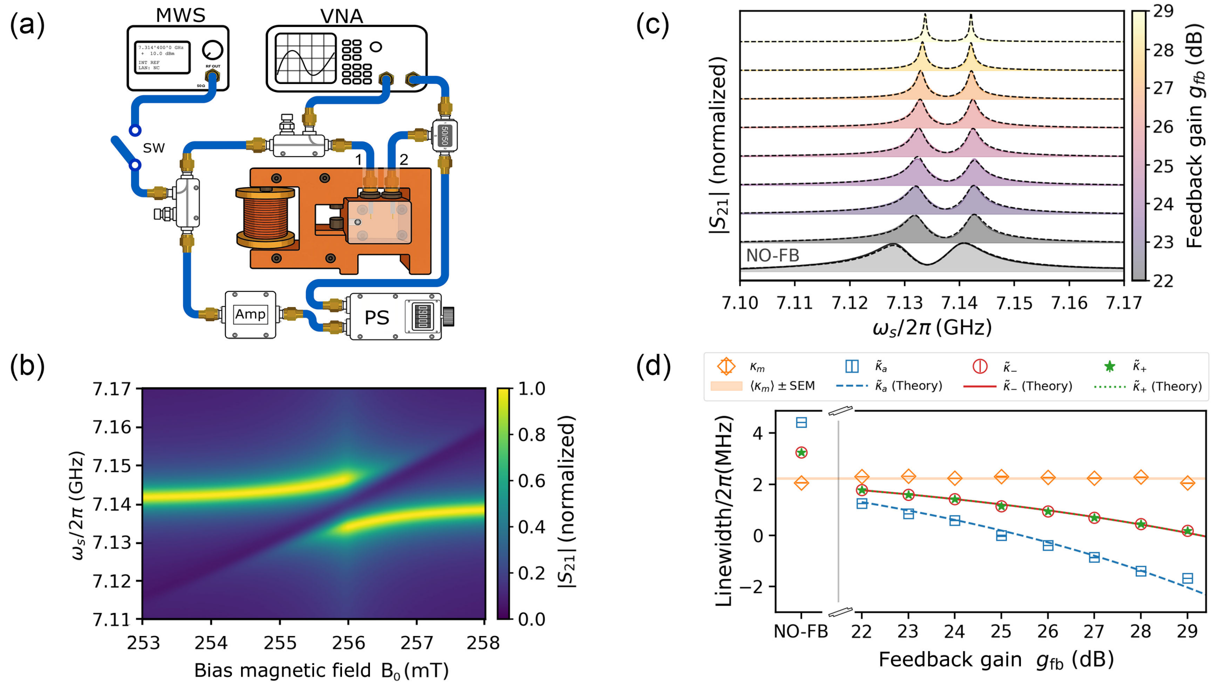

FIG. 1. Feedback reduces the hybridized polariton dissipation below the magnon linewidth. (a) Simplified schematic of the cavity magnomechanical system and microwave feedback loop. The copper cavity is surrounded by a tunable magnet and probed by a vector network analyzer (VNA) through port 1. A fraction of the cavity output (port 2) is directed to the VNA for measurement, while the remaining signal is routed through the feedback loop. In the feedback loop, the signal is phase shifted (PS), amplified (Amp), and subsequently fed back into the cavity through port 1. A pump tone can be added to the circuit using an independent microwave source (MWS). (b) Polariton spectra demonstrating strong coupling between magnons and cavity photons as the bias field is tuned. (c) Transmission amplitude of the cavity-magnon polariton modes with increasing feedback gain $g_{\rm fb}$. Each trace is normalized and vertically offset for clarity. For each spectrum, the bias magnetic field was adjusted to maintain symmetric polariton modes. In the absence of feedback (NO-FB), the system exhibits broad hybrid modes, while increasing feedback gain progressively narrows the polariton linewidths. (d) Extracted linewidths of the upper ($\tilde{\kappa}_+$) and lower ($\tilde{\kappa}_-$) polariton modes, together with the intrinsic magnon dissipation rate κ_m and the effective cavity linewidth $\tilde{\kappa}_a$, as functions of the feedback gain $g_{\rm fb}$. The shaded orange band indicates the uncertainty in the fits to the magnon linewidths, shown as the mean value $\langle\kappa_m\rangle \pm$ SEM, where SEM denotes the standard error of the mean. The feedback-induced linewidth reduction suppresses the polariton dissipation more than an order of magnitude below the magnon-limited linewidth.

photon-magnon interaction [10,38]. The introduction of an active microwave feedback loop alters the cavity response by effectively modifying its resonance frequency to

$$\tilde{\omega}_a \equiv \omega_a + 2\sqrt{\eta\kappa_{\rm ext}^{(1)}\kappa_{\rm ext}^{(2)}}g_{\rm fb}\sin\phi, \tag{1}$$

and its decay rate to

$$\tilde{\kappa}_a \equiv \kappa_a - 2\sqrt{\eta\kappa_{\rm ext}^{(1)}\kappa_{\rm ext}^{(2)}}g_{\rm fb}\cos\phi. \tag{2}$$

In Eqs. (1), (2), whose detailed theoretical derivations are provided in Appendices 1 B and 1 C, the total cavity decay is $\kappa_a = \kappa_{\rm int} + \kappa_{\rm ext}^{(1)} + \kappa_{\rm ext}^{(2)}$, which is composed of the intrinsic contribution $\kappa_{\rm int}$ and the decay into two external ports $\kappa_{\rm ext}^{(1,2)}$. The parameters $g_{\rm fb}$ and ϕ are the feedback gain and feedback phase, respectively, both of which can be experimentally tuned. Here, η denotes the effective feedback-loop efficiency, which characterizes the net coherent transmission between the cavity output and the feedback input. This parameter accounts for the combined effects of insertion losses, impedance mismatches, and other imperfections throughout the microwave feedback circuit. Experimentally, η is determined from an independent calibration of the complete feedback loop, as described in Appendix 2 A.

Correspondingly, the magnon-microwave polaritons exhibit modified frequencies $\tilde{\omega}_\pm$ and decay rates $\tilde{\kappa}_\pm$, obtained by diagonalizing the linear Heiseberg-Langevin equations governing the coupled mode dynamics (see Appendix 1). In the simpler case where the magnon frequency ω_m is adjusted to always be on resonance with the feedback modified cavity frequency $\tilde{\omega}_a$, the polaritons frequencies and decays are given by

$$\tilde{\omega}_\pm = \tilde{\omega}_a \pm \sqrt{g_{ma}^2 - (\tilde{\kappa}_a - \kappa_m)^2/4}, \tag{3}$$

$$\tilde{\kappa}_{\pm} = (\tilde{\kappa}_a + \kappa_m)/2, \tag{4}$$

where we have also assumed that $g_{ma} > |\tilde{\kappa}_a - \kappa_m|/2$, which is always the case for our experiment.

The strong photon-magnon hybridization implies that the feedback provides direct control over the properties of the hybrid cavity-magnon polariton modes, as we can infer from Eqs. (4) and (2): for $-\pi/2 < \phi < \pi/2$, the effective polariton linewidths $\tilde{\kappa}_{\pm}$ are always reduced in comparison with the no-feedback case. The optimum feedback phase is $\phi = 0$, which yields, at a fixed gain, the maximum reduction of the polariton linewidths. In this regime, the gain introduced by the feedback loop compensates for intrinsic dissipation in the system. We engineer this scenario with our setup and probe the transmission of the system, which we show in Fig. 1(c) for different feedback gains. As the feedback gain is increased, a pronounced narrowing of the polariton resonances is observed, indicating a strong suppression of the effective polariton dissipation. Small deviations of the phase from zero can lead to frequency shifts at high gain values. To compensate for these shifts and maintain symmetric polariton splitting throughout the measurement sequence, the bias magnetic field was manually adjusted for each spectrum. This enables a consistent comparison of linewidth suppression across different feedback gains. It is noteworthy that while the symmetric polariton configuration is used in Fig. 1(c), even narrower linewidths can be achieved for one of the polariton modes through intentional polariton linewidth asymmetry (see Sec. III), at the expense of increased dissipation in the second mode.

The experimental data can be explained and fit using the theoretical model developed in Appendix 1. From standard input-output relations, we obtain the scattering matrix describing the reflection and transmission amplitude from the input to the output ports. The transmission amplitude from port 1 to port 2 is given by

$$S_{21}[\omega_s] = \frac{2\sqrt{\kappa_{\mathrm{ext}}^{(1)}\kappa_{\mathrm{ext}}^{(2)}}\tilde{\chi}_a[\omega_s]}{1 + \chi_m[\omega_s]\tilde{\chi}_a[\omega_s]g_{ma}^2}, \tag{5}$$

where ω_s is the swept VNA probe frequency, $\chi_m[\omega_s] = [\kappa_m + i(\omega_m - \omega_s)]^{-1}$ is the magnon susceptibility, and $\tilde{\chi}_a[\omega_s] = [\tilde{\kappa}_a + i(\tilde{\omega}_a - \omega_s)]^{-1}$ shows the effective cavity susceptibility in the presence of feedback. The transmission coefficient, S_{21}, characterizes the resonant response of the system. The poles of Eq. (5) are directly related to the polariton frequency and linewidth. The absolute value $|S_{21}[\omega_s]|$, for the parameter regime of interest, has the shape of two Lorentzians with peak frequencies and linewidths corresponding to the frequencies and linewidths of the polariton modes. We then use Eq. (5) to fit our experimental data, shown in Fig. 1(c). The model, shown in dashed lines, exhibits excellent agreement with the experimental data. From these fits, the polariton linewidths (at the maximally hybridized, symmetric polariton point) extracted using Eq. (4) are reduced from approximately 3.24 MHz in the absence of feedback to as low as 174 kHz at the highest feedback gain, thereby overcoming the intrinsic magnon dissipation rate, $\kappa_m/2\pi = 2.20$ MHz, Fig. 1(d). The experimental results presented in Sec. III correspond to the asymmetric polariton regime, in which the linewidth of the narrower polariton mode can be suppressed to as low as 300 Hz. This demonstrates that intrinsic material-limited dissipation can be overcome through feedback.

Figure 1(d) shows the extracted dissipation parameters, including the effective cavity decay rate, $\tilde{\kappa}_a$, the intrinsic magnon dissipation rate, κ_m, and the polariton decay rates, $\tilde{\kappa}_{\pm}$, obtained from Eq. (4). The formally negative effective cavity decay rate $\tilde{\kappa}_a$ does not by itself imply instability of the system, rather indicating that the cavity mode behaves as an amplifying subsystem [44,47]. Since the cavity is strongly coupled to the magnon mode, which is also dissipative, the linear stability of the system is guaranteed by the positiveness of the polariton decay rates, which is always the case in our measurements. Note however, this would not be the case for the bare cavity, which is investigated in Appendix 2 B. There, we show that at sufficiently high feedback gain the bare cavity becomes unstable, resulting in distorted transmission spectra.

III. FEEDBACK-ENABLED STRONG MAGNOMECHANICAL COUPLING

The radiation-pressure-like magnon-phonon interaction in cavity magnomechanics manifests experimentally through interference effects in the probe response. The analog of optomechanically induced transparency/absorption in cavity optomechanics [72]—known as magnomechanically induced transparency/absorption (MMIT/MMIA)—arises from coherent interference between the weak probe field and the anti-Stokes (Stokes) scattering generated by a strong red- (blue-) detuned control field via mechanical motion. This interference produces a narrow transparency window or absorption dip in the probe transmission near the polariton resonance, with a linewidth set by the mechanical dissipation rate [15,16]. In this section, we investigate this effect, which provides a sensitive probe of the magnomechanical coupling.

A key figure of merit characterizing the interaction between the polariton and mechanical modes is the polariton-phonon cooperativity,

$$C = \frac{G_+^2}{\tilde{\kappa}_+\kappa_b}, \tag{6}$$

where G_+ denotes the cavity-enhanced polariton-phonon coupling strength, $\tilde{\kappa}_+$ is the effective upper-polariton dissipation rate, and κ_b is the mechanical dissipation rate.

The relatively large linewidth of cavity-magnon polaritons constitutes a major obstacle to reaching the strong-coupling regime and, because the cooperativity is inversely proportional to the polariton dissipation rate, also hinders further enhancement of the cooperativity. Consequently, increasing the drive power alone is generally insufficient to substantially enhance the cooperativity. Moreover, further increases in drive power may introduce unwanted heating and nonlinearities, motivating alternative strategies for increasing the cooperativity.

The MMIT response of the upper polariton mode in cavity magnomechanics, realized using a YIG sphere with a mechanical resonance frequency of $\omega_b/2\pi = 15.61$ MHz, a single-magnon-phonon coupling rate $g_{mb}/2\pi = 4.83$ mHz, and an intrinsic mechanical linewidth $\kappa_b/2\pi = 2.06$ kHz, without the feedback loop is shown in Fig. 2(b). As the drive is tuned to the red side of the upper polariton mode [see Fig. 2(a)], a small transparency window appears at the top of the upper polariton resonance. The weak magnetostrictive magnon-phonon interaction, together with the intrinsically large polariton linewidth prevents the formation of a wide transparency window. As the results in Fig. 2(b) show, even increasing the drive power up to 20 dBm is insufficient to observe cavity-magnon polariton mechanical normal-mode splitting. This is a direct consequence of an intrinsic limitation of the system—the decay rates prevent the magnomechanical cooperativity to be increased solely via a stronger drive.

Motivated by the experimentally demonstrated feedback-enabled polariton linewidth narrowing, we now investigate the interaction between magnon-microwave polaritons and phonons in a cavity magnomechanical system inside the feedback loop. In the following, in addition to the feedback circuit above, a drive tone is applied to port 1 using a directional coupler [Fig. 1(a) with switch closed]. This tone is tuned to the red sideband of the

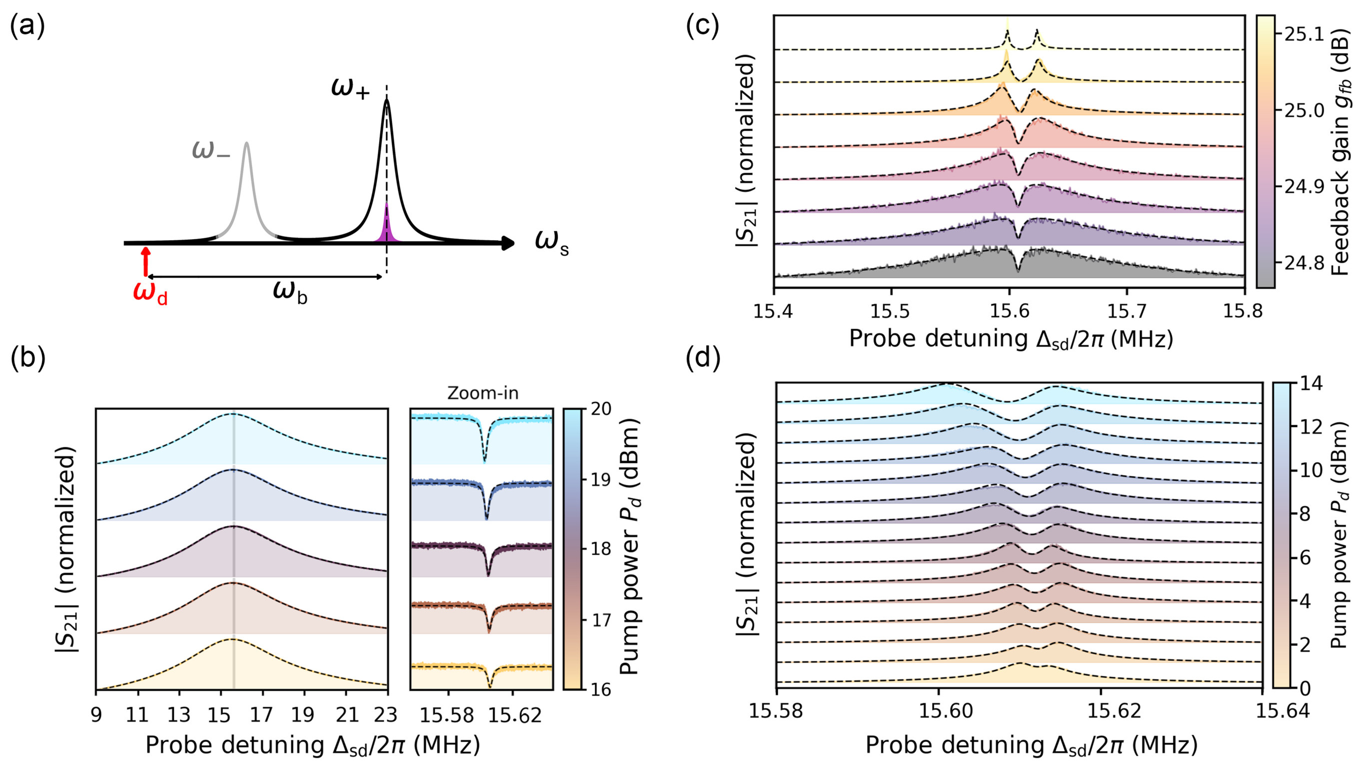

FIG. 2. Feedback-induced strong magnomechanical coupling. (a) Frequency schematic of the measurement showing the pump tone, ω_d, approximately one mechanical frequency, ω_b, red-detuned from the upper polariton mode, ω_+. (b) Transmission amplitude, $|S_{21}|$, of the upper cavity-magnon polariton as a function of the probe detuning $\Delta_{sd} = \omega_s - \omega_d$ in the absence of feedback. As the red-detuned pump tone is increased, a transparency peak appears, reflecting interference with the mechanical resonance arising from the cavity-enhanced coupling. Despite the increasing drive power, the transparency feature remains small and no normal-mode splitting is observed. (c) When feedback gain is applied, there is a clear transparency peak that evolves into a well-defined normal mode splitting as the gain is increased (with constant pump tone power, $P_d = 18$ dBm). (d) Transmission amplitude, $|S_{21}|$, of the upper cavity-magnon polariton measured as a function of increasing pump power (bottom to top) inside the microwave feedback-loop, shown for direct comparison with the no-feedback measurements in panel (b). The feedback gain is fixed at $g_{\mathrm{fb}} = 27$ dB and the feedback phase is tuned to $\phi \simeq 0$, corresponding to the regime of maximum polariton linewidth suppression. In contrast to panel (b), where increasing pump power alone does not produce resolvable normal-mode splitting, the feedback induced linewidth suppression enables the drive-enhanced magnomechanical interaction to overcome the dissipation rates, leading to the emergence of normal-mode splitting. Dashed lines represent fits to the theoretical model.

upper polariton mode and the drive power is fixed at 18 dBm, for which the mechanically induced transparency window is not clearly visible in the setup without the feedback loop. Under these otherwise identical conditions, we examine the effect of feedback on the MMIT response.

Figure 2(c) shows the MMIT spectra measured at different feedback gains, fixed optimum phase $\phi \simeq 0$, and a red-detuned drive at a fixed power of $P_d = 18$ dBm. As the feedback gain is increased, the progressive suppression of the polariton linewidth enables the emergence of a clear normal-mode splitting. This splitting provides direct evidence for the onset of the strong-coupling regime between the polariton mode and the phonon mode. Because increasing the feedback gain shifts the polariton resonance frequency, the external bias field is adjusted during the measurement sequence to maintain the hybrid polariton-phonon modes near symmetric mode splitting. The adjustment is performed manually by monitoring the polariton spectrum and maintaining an approximately symmetric normal-mode splitting about the center frequency, with a typical field correction of less than $\sim$0.05, mT. This procedure ensures that the observed normal-mode splitting arises from enhanced magnomechanical coupling rather than from frequency detuning-induced asymmetry.

For direct comparison with the no-feedback measurements shown in Figs. 2(b) and 2(d) presents the corresponding transmission spectra measured under otherwise identical conditions with the feedback loop enabled. In these measurements, the feedback gain is fixed at $g_{\mathrm{fb}} = 27$ dB and the feedback phase is tuned to $\phi \simeq 0$, corresponding to the regime of maximum polariton linewidth suppression. Under these conditions, the feedback-induced reduction of the polariton linewidth allows the drive-enhanced magnomechanical interaction to overcome the dissipation rates, resulting in the clear emergence of normal-mode splitting. A comparison of Figs. 2(b) and 2(d) demonstrates that increasing the drive power alone is insufficient to reach the strong-coupling regime. Instead, the feedback-enabled suppression of the polariton linewidth is the key mechanism that enables coherent polariton-mechanical hybridization.

Driving the upper polariton mode in the red-detuned regime, $\omega_d = \tilde{\omega}_+ - \omega_b$, the transmission amplitude describing the upper polariton-mechanical interaction is given by

$$S_{21}[\Delta_{sd}] = \frac{2\sqrt{\tilde{\kappa}^{(1)}_{+,\mathrm{ext}}\kappa^{(2)}_{\mathrm{ext}}}\tilde{\chi}_+[\Delta_{sd}]}{1 + \chi_b[\Delta_{sd}]\tilde{\chi}_+[\Delta_{sd}]|G_+|^2}, \tag{7}$$

where $\tilde{\kappa}^{(1)}_{+,\mathrm{ext}}$ is the effective external coupling rate of the upper polariton to port 1 [see Eq. (A25) in Appendix 1], $\tilde{\chi}_+[\Delta_{sd}] = [\tilde{\kappa}_+ + i(\omega_b - \Delta_{sd})]^{-1}$ and $\chi_b[\Delta_{sd}] = [\kappa_b + i(\omega_b - \Delta_{sd})]^{-1}$ denote the effective upper polariton and mechanical susceptibilities, respectively, $\Delta_{sd} = \omega_s - \omega_d$ is the probe-drive detuning, and G_+ represents the effective upper-polariton-phonon coupling strength. Such a transmission amplitude probes the response of the system which, just as in the case of Sec. II, exhibits a resonant behavior at the polariton mode frequency, including a suppression due to MMIT in the weak coupling and mode splitting in the strong coupling regime. This behavior can be seamlessly tuned by varying the feedback gain g_{fb}. Alternatively, for a fixed feedback gain, it can be controlled by increasing the drive power, which enhances the effective upper-polariton-phonon coupling strength G_+ (see Appendix 1 E). The fit theoretical spectra obtained from Eq. (7), shown as black dashed lines in Figs. 2(c) and 2(d), exhibit excellent agreement with the experimental data. To provide a more comprehensive comparison, the same experimental and theoretical data shown in Fig. 2(c) are displayed as two-dimensional contour plots in Appendix 2 A.

To quantitatively analyze the measured spectra in Fig. 2(c), each spectrum is fit using the theoretical model described by Eq. (7). In the fitting procedure, the product of the external dissipation rates, $\tilde{\kappa}^{(1)}_{+,e}\kappa^{(2)}_{\mathrm{ext}}$, is fixed to independently calibrated values, while the effective upper-polariton dissipation rate $\tilde{\kappa}_+$, the mechanical dissipation rate κ_b, the cavity-enhanced polariton-phonon coupling strength G_+, and the mechanical resonance frequency ω_b are treated as free fitting parameters. The resulting theoretical fits, shown as black dashed lines in Fig. 2(c), reproduce the measured line shapes with excellent agreement over the entire feedback-gain range, confirming that Eq. (7) accurately captures the feedback-modified polariton-phonon dynamics. The fit parameters are summarized in Fig. 3(a). To clarify the possibility of strong coupling, only the extracted values of $\tilde{\kappa}_+$, κ_b, and G_+ are displayed. Because the red-sideband drive power is fixed at $P_d = 18$ dBm, both the cavity-enhanced coupling strength G_+ and the mechanical dissipation rate κ_b depend on the feedback gain only weakly. In contrast, the effective upper-polariton dissipation rate, $\tilde{\kappa}_+/2\pi$, decreases substantially with increasing feedback gain, from $\tilde{\kappa}_+/2\pi = 74$ kHz at $g_{\mathrm{fb}} = 24.77$ dB to $\tilde{\kappa}_+/2\pi \approx 300$ Hz at $g_{\mathrm{fb}} = 25.12$ dB, demonstrating the feedback-induced suppression of polariton damping. The extracted parameters provide a quantitative criterion for identifying the onset of strong coupling. At sufficiently high feedback gain, the system satisfies the condition $G_+ > \tilde{\kappa}_+, \kappa_b$, indicated by the shaded region in Fig. 3(a). While the emergence of normal-mode splitting is already evident in Figs. 2(c), the parameters in Fig. 3(a) explicitly identify the strong-coupling threshold.

Finally, the polariton-mechanical cooperativity, $C = G_+^2/\tilde{\kappa}_+\kappa_b$, which quantifies the competition between coherent coupling and dissipation, is shown in Fig. 3(b). While at low feedback gain the cooperativity is of order unity ($C \simeq 1$), increasing the feedback gain enables

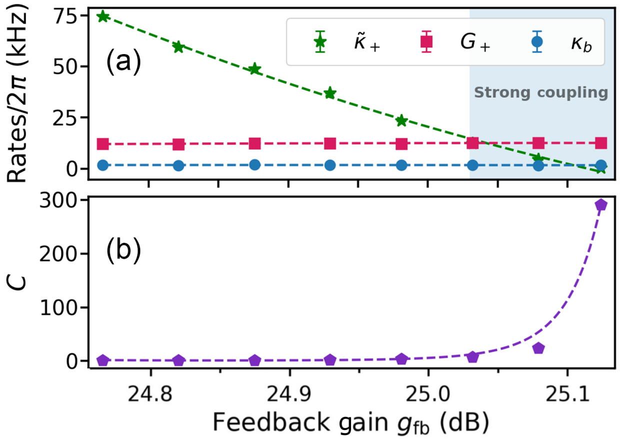

FIG. 3. Extracted parameters characterizing the feedback-induced strong-coupling regime. (a) Coupling and dissipation rates extracted from fits to the transmission amplitude shown in Fig. 2(b) as functions of the feedback gain g_{fb}. The effective polariton-mechanical coupling strength G_+ and the mechanical dissipation rate κ_b remain approximately constant, while the effective upper-polariton linewidth $\tilde{\kappa}_+$ is strongly suppressed with increasing feedback gain. The blue shaded region highlights the parameter range in which the strong-coupling condition $G_+ > \tilde{\kappa}_+, \kappa_b$ is satisfied. (b) Polariton-mechanical cooperativity $C = G_+^2/(\tilde{\kappa}_+ \kappa_b)$ calculated from the extracted rates as a function of the feedback gain g_{fb}, showing a significant enhancement driven by feedback-induced linewidth suppression.

cooperativities as large as $C \simeq 300$. This large cooperativity establishes the cavity magnomechanical system as a promising platform for coherent quantum operations, including mechanical cooling and microwave/magnon-mechanical quantum transduction [51,52,61–64,73–76].

Having established the feedback-induced strong-coupling regime through linewidth suppression, which consequently enhances the polariton-phonon cooperativity, we now present direct spectroscopic evidence of coherent hybridization between the upper polariton mode and the mechanical resonance. Figure 4 shows the transmission amplitude of a weak probe with frequency ω_s with a strong drive at a frequency ω_d red-detuned with respect to the upper polariton. The double peaked structure indicates polariton-phonon hybridization. As the drive frequency is swept across the red-detuned regime of the upper polariton resonance, a clear avoided crossing emerges, which is a hallmark of coherent mode hybridization and cannot be explained by interference or linewidth narrowing alone. At the red-sideband condition, the transmission transforms from a single resonance into two well-resolved peaks accompanied by a characteristic dispersive phase response, providing unambiguous evidence of normal-mode splitting arising from coherent polariton-mechanical coupling.

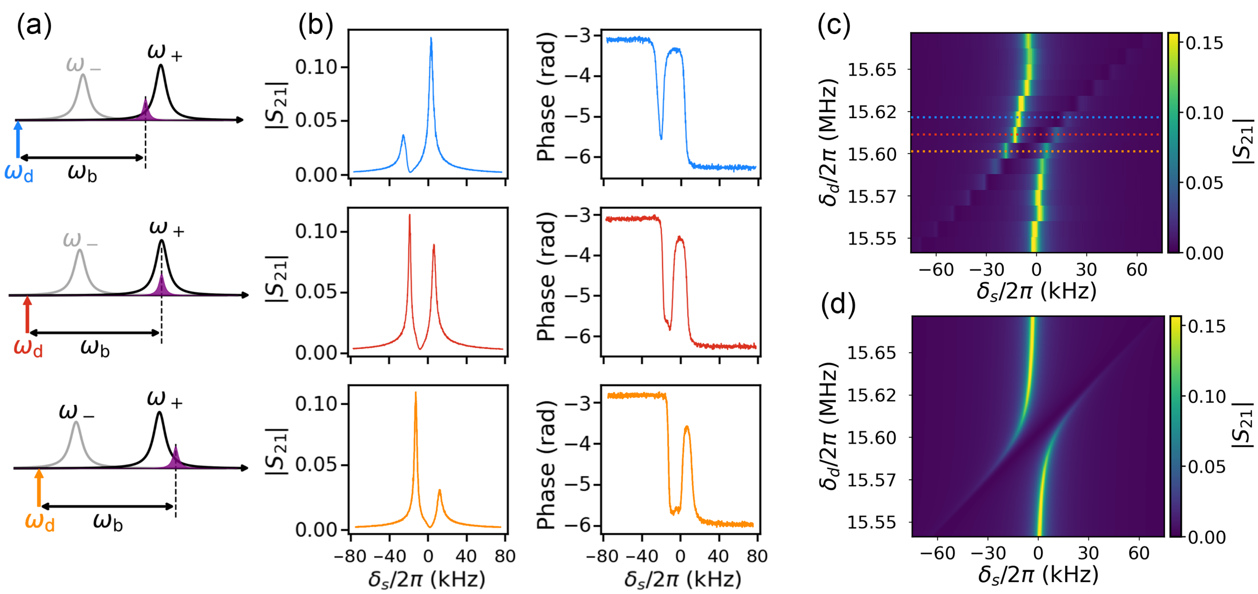

FIG. 4. Normal-mode (avoided level crossing) spectrum of the upper polariton-mechanical system enabled by feedback-induced linewidth suppression. Unless otherwise stated, the measurements are performed at a fixed probe power of $P_d = 15$, dBm, feedback gain $g_{\mathrm{fb}} = 29.75$, dB, and feedback phase $\phi \simeq 0$. (a) Schematic diagrams illustrating the relative positions of the lower and upper polariton modes (ω_-, ω_+), the drive/pump tone ω_d, and the mechanical frequency ω_b for three representative drive frequencies (blue, orange, and red). (b) Corresponding line cuts of the transmission amplitude $|S_{21}|$ (left column) and phase (right column) measured at the three drive frequencies indicated in panel (a), plotted as functions of the probe detuning $\delta_s = \omega_s - \omega_0$, where $\omega_0/2\pi$ denotes the center frequency of each measurement sweep (roughly ω_+). The evolution from a single resonance into two well-resolved peaks, accompanied by the characteristic phase response, reveals normal-mode splitting in the strong-coupling regime. (c) Experimental color map of the transmission amplitude $|S_{21}|$ as a function of the probe and drive detunings, $\delta_s = \omega_s - \omega_0$ and $\delta_d = \omega_0 - \omega_d$. The clear avoided crossing demonstrates coherent hybridization between the upper polariton mode and the mechanical resonance. Colored dotted lines indicate the three drive frequencies corresponding to the line cuts shown in panel (b). (d) Theoretical simulation of the transmission amplitude $|S_{21}|$ plotted in the same detuning coordinates (δ_s, δ_d), showing excellent agreement with the experimentally observed avoided-crossing spectrum.

IV. CONCLUSION

In this work, we have experimentally demonstrated that active microwave feedback can overcome intrinsic material dissipation in cavity magnomechanics, the main limiting factor in practical applications. By implementing a tunable feedback loop that modifies the effective dissipation of cavity-magnon polariton modes, we achieve a substantial suppression of the polariton linewidth to below the magnon-limited linewidth. This linewidth engineering enables the effective polariton-phonon coupling strength to exceed the total system decay rates, thereby allowing the system to enter the magnomechanical strong-coupling regime.

As a direct consequence, we observe clear normal-mode splitting between a cavity-magnon polariton and a mechanical mode, providing conclusive spectroscopic evidence of coherent hybridization among photons, magnons, and phonons. Control measurements performed under identical drive conditions but without feedback confirm that increasing the drive power alone is insufficient to reach this regime, demonstrating that feedback-enabled linewidth suppression is the key mechanism enabling strong magnomechanical coupling.

Beyond the implementation presented here, our results establish feedback-enabled linewidth engineering as a general strategy for accessing strongly coupled regimes in hybrid magnonic platforms that are otherwise limited by intrinsic magnetic losses and weak single-magnon magnomechanical coupling rates. This approach opens new opportunities for the realization of coherent information transfer [20,25,76], quantum-limited control of mechanical motion [51,52,61–64,73–76], microwave-magnon-mechanical transduction [25,77], feedback-controlled non-Hermitian and exceptional-point physics in hybrid quantum systems [21,29,48], and generation of entanglement between two remote mechanical resonators [20]. For such implementations in the quantum regime, it will be important to benchmark the noise introduced in the system by the feedback loop, which is known to limit, for example, the cooling performance of feedback-schemes in optomechanics [53,60,78]. Even with such added noise, feedback cooling and squeezing schemes in optics and microwave-based systems are known to enable quantum control [53], which we also anticipate to be the case in this system.

ACKNOWLEDGMENTS

The authors acknowledge that the land on which this work was performed is on Treaty Six Territory, the traditional lands of many First Nations, Métis, and Inuit in Alberta. They acknowledge the support from the Natural Sciences and Engineering Research Council, Canada (Grants No. RGPIN-2022-03078, No. ALLRP 592535-23, No. ALLRP 568609-21); Alberta Innovates (Grant No. 212200780); the National Research Council (Grant No. QSP-017-1); and the University of Alberta Department of Physics through the Advah Bhatia Fellowship. A. M. and V. A. S. V. Bittencourt acknowledge funds from the Agence nationale de la recherche, France (Grant No. A25R321A/2025DRI00103 "FeEnQCaMM"). V. A. S. V. Bittencourt thanks C. A. Potts (University of Calgary) for useful discussions.

DATA AVAILABILITY

The data that support the findings of this article are not publicly available upon publication because it is not technically feasible and/or the cost of preparing, depositing, and hosting the data would be prohibitive within the terms of this research project. The data are available from the authors upon reasonable request.

APPENDIX A: THEORETICAL BACKGROUND

1. Basic cavity magnon system

Magnons and microwaves couple via a magnetic-dipole dipole interaction, and can be made close in frequency, allowing for coherent exchange of energy. Microwave cavities can be engineered to exhibit electromagnetic modes at well-defined and separated frequencies, such as the TE_{101} mode used here we can consider the interaction between a magnon mode, with annihilation operator $\hat{m}$ and frequency ω_m, and a single cavity mode, described with the annihilation operator $\hat{a}$ and frequency ω_a. The Hamiltonian of the cavity-magnon system is given by

$$\frac{\hat{H}}{\hbar} = \omega_a \hat{a}^\dagger \hat{a} + \omega_m \hat{m}^\dagger \hat{m} + g_{ma}(\hat{m}\hat{a}^\dagger + \hat{a}\hat{m}^\dagger) + i\sqrt{2\kappa_{\mathrm{ext}}^{(1)}}\varepsilon_s(\hat{a}^\dagger e^{-i\omega_s t} - \hat{a}e^{i\omega_s t}), \tag{A1}$$

where the last term describes a coherent monochromatic drive with amplitude ε_s applied via an external port that couples to the microwave mode with a rate $\kappa_{\mathrm{ext}}^{(1)}$. The magnon-microwave coupling rate g_{ma} depends on the system architecture [36,79].

In our experiment, the microwave resonator is a 3D cavity, supporting a fundamental TEM_{101} mode, and the magnet hosting the magnons is a yttrium iron-garnet sphere with a diameter much smaller than the wavelength of the fundamental mode of the cavity. In this case, the magnon-microwave coupling depends on the position of the sphere inside the cavity and its volume [10]. Systems like the one used in this experiment can routinely achieve strong magnon-microwave coupling [10,12,36,38], which results in the formation of magnon-microwave polaritons [36,38].

The quantum Langevin equations (QLEs) describing the system dynamics are

$$\dot{\hat{a}} = (-i\omega_a - \kappa_a)\hat{a} - ig_{ma}\hat{m} + \sqrt{2\kappa_a}\hat{\mathcal{A}}_{\rm in} + \sqrt{2\kappa_{\rm ext}^{(1)}}\varepsilon_s e^{-i\omega_s t}, \tag{A2a}$$

$$\dot{\hat{m}} = (-i\omega_m - \kappa_m)\hat{m} - ig_{ma}\hat{a} + \sqrt{2\kappa_m}\hat{m}_{\rm in}, \tag{A2b}$$

where κ_a and κ_m denote the total decay rates of the cavity and magnon modes, respectively, $\kappa_{\rm ext}^{(1)}$ is the external coupling rate through cavity port 1. The noise operator $\hat{m}_{\rm in}$ describes vacuum and thermal noise acting on the magnon mode, while $\hat{\mathcal{A}}_{\rm in}$ includes both intrinsic cavity noise, and noise fed to the cavity via its input ports.

Throughout these appendices, we will indicate the coherent part of the fields as, e.g., $a = \langle\hat{a}\rangle$. We further consider white noise exclusively, such that $\langle\hat{m}_{\rm in}\rangle = \langle\hat{\mathcal{A}}_{\rm in}\rangle = 0$.

2. Microwave feedback

We now introduce a feedback loop acting on the cavity mode. As illustrated schematically in Fig. 1(a), the output field from one port of the cavity (port 2) is amplified, phase shifted, and then fed back into the cavity through port 1, which is also used to apply the probe field. The coherent amplitude of the input field at port 1 is therefore given by

$$a_{\rm in}^{(1)}(t) = \varepsilon_s + \sqrt{\eta}g_{fb}a_{\rm out}^{(2)}(t - \tau_{fb}), \tag{A3}$$

where g_{fb} is the feedback gain, η denotes the efficiency of the feedback loop, and τ_{fb} is the feedback delay time. The feedback also adds contributions to the noise term $\hat{\mathcal{A}}_{\rm in}$ appearing in Eq. (A2). We indicate the modified noise contributions by $\hat{\tilde{\mathcal{A}}}_{\rm in}$.

When the delay time is much shorter than both the cavity lifetime $1/\kappa_a$ and the characteristic interaction time $1/g_{ma}$, its effect can be absorbed into an effective phase shift, which allows us to write the coherent part of the input as

$$a_{\rm in}^{(1)}(t) = \varepsilon_s + \sqrt{\eta}g_{fb}a_{\rm out}^{(2)}(t)e^{-i\phi}, \tag{A4}$$

where

$$\phi \equiv \theta_{fb} + (\omega_a - \omega_s)\tau_{fb} \tag{A5}$$

is the total feedback phase, with θ_{fb} controlled externally. Taking the feedback into account and using standard input-output theory [80], the output field from port 2, with external coupling $\kappa_{\rm ext}^{(2)}$, is given by

$$\hat{a}_{\rm out}^{(2)}(t) = \sqrt{2\kappa_{\rm ext}^{(2)}}\hat{a}(t) + \hat{a}_{\rm in}^{(2)}(t). \tag{A6}$$

We emphasize that in our experiment, no coherent drive is applied via port 2, hence $\hat{a}_{\rm in}^{(2)}$ is composed of only thermal and vacuum noise.

The cavity quantum Langevin equation is therefore modified to

$$\dot{\hat{a}} = (-i\omega_a - \kappa_a)\hat{a} - ig_{ma}\hat{m} + \sqrt{2\kappa_{\rm ext}^{(1)}}\left(\varepsilon_s + \sqrt{2\eta\kappa_{\rm ext}^{(2)}}g_{fb}\hat{a}e^{-i\phi}\right)e^{-i\omega_s t} \tag{A7}$$

$$+\sqrt{2\kappa_a}\hat{\tilde{\mathcal{A}}}_{\rm in}, \tag{A8}$$

Equation (A8) explicitly shows that the feedback loop introduces an effective self-interaction of the cavity field through coherent extraction, processing, and reinjection of the intracavity field.

3. Effective cavity parameters

The feedback-induced self-interaction can be absorbed into renormalized cavity parameters. We can thus rewrite Eq. (A8) for the coherent amplitude of the cavity as

$$\dot{a} = (-i\tilde{\omega}_{\rm a} - \tilde{\kappa}_{\rm a})a - ig_{ma}m + \sqrt{2\kappa_{\rm ext}^{(1)}}\varepsilon_s e^{-i\omega_s t}. \tag{A9}$$

The effective cavity frequency and decay rate are given by

$$\tilde{\omega}_a \equiv \omega_a + 2\sqrt{\eta\kappa_{\rm ext}^{(1)}\kappa_{\rm ext}^{(2)}}g_{fb}\sin\phi, \tag{A10}$$

$$\tilde{\kappa}_a \equiv \kappa_a - 2\sqrt{\eta\kappa_{\rm ext}^{(1)}\kappa_{\rm ext}^{(2)}}g_{fb}\cos\phi. \tag{A11}$$

We emphasize that the feedback loop acts exclusively on the cavity mode, leaving the intrinsic magnon parameters ω_m and κ_m unchanged. By tuning the feedback gain and phase, the effective cavity frequency and decay rate can be continuously engineered, enabling controlled enhancement or suppression of cavity dissipation.

Nonlinear effects, such as those discussed in Ref. [44], are expected to be negligible under the operating conditions of the present experiment. To verify this assumption, we performed additional measurements of the cavity-feedback system while varying the VNA probe power. The resonance frequency, linewidth, and overall line shape exhibited only weak dependence on probe power, indicating that the system remains well within the linear-response regime. Consequently, the effective cavity dynamics are well described by the linear model presented here.

4. Feedback-controlled polariton modes

Because the cavity and magnon modes are strongly coupled, it is convenient to describe the system in terms of hybrid cavity-magnon polaritons. The QLEs for the magnon and cavity coherent amplitudes in the presence of feedback read

$$\dot{a} = (-i\tilde{\omega}_a - \tilde{\kappa}_a)a - ig_{ma}m + \sqrt{2\kappa_{\rm ext}^{(1)}}\varepsilon_s e^{-i\omega_s t}, \quad \text{(A12a)}$$

$$\dot{m} = (-i\omega_m - \kappa_m)m - ig_{ma}a. \quad \text{(A12b)}$$

The complex eigenfrequencies of the hybrid polariton modes are given by

$$\tilde{\omega}_\pm - i\tilde{\kappa}_\pm = \frac{\tilde{\omega}_a + \omega_m}{2} - i\frac{\tilde{\kappa}_a + \kappa_m}{2} \pm \sqrt{g_{ma}^2 + \left(\frac{\tilde{\omega}_a - \omega_m}{2} - i\frac{\tilde{\kappa}_a - \kappa_m}{2}\right)^2}, \quad \text{(A13)}$$

where $\tilde{\omega}_\pm$ and $\tilde{\kappa}_\pm$ denote the resonance frequencies and dissipation rates of the hybrid polariton modes, respectively. The corresponding hybrid polariton modes are given by

$$\begin{pmatrix} \hat{A}_+ \\ \hat{A}_- \end{pmatrix} = \begin{pmatrix} \cos\psi & \sin\psi \\ -\sin\psi & \cos\psi \end{pmatrix} \begin{pmatrix} \hat{a} \\ \hat{m} \end{pmatrix}, \quad \text{(A14)}$$

where the mixing angle ψ is defined by

$$\tan(2\psi) = \frac{2g_{ma}}{\omega_m - \tilde{\omega}_a}. \quad \text{(A15)}$$

Equation (A13) shows that, in general, the polariton linewidths, $\tilde{\kappa}_\pm$, are governed by the feedback-modified cavity parameters. For analytical transparency, we consider the resonant case $\tilde{\omega}_a = \omega_m$, where the linewidths reduce to

$$\tilde{\kappa}_\pm = \frac{\tilde{\kappa}_a + \kappa_m}{2} = \frac{\kappa_a - 2\sqrt{\eta\kappa_{\rm ext}^{(1)}\kappa_{\rm ext}^{(2)}}g_{fb}\cos\phi + \kappa_m}{2}. \quad \text{(A16)}$$

Equation (A16) demonstrates that, although intrinsic magnon dissipation typically dominates cavity magnonic systems and limits the polariton lifetime, appropriately engineered microwave feedback allows direct control over the effective polariton dissipation. By tuning the feedback gain and phase, the cavity mode can be driven into a regime of reduced or even negative effective dissipation, effectively behaving as an amplifying mode. When hybridized with the lossy magnon mode, this feedback-induced amplification compensates the magnon dissipation, resulting in a pronounced suppression of the polariton linewidth. In the ideal limit, and within the stability bounds of the feedback loop, the polariton linewidth can be made arbitrarily small.

To obtain the transmission amplitude given in Eq. (5), we use the standard input-output relations

$$\hat{a}_{\rm out}^{(i)}(t) = \hat{a}_{\rm in}^{(i)}(t) + \sqrt{2\kappa_{\rm ext}^{(i)}}\hat{a}(t), \qquad (i = 1, 2). \quad \text{(A17)}$$

We should notice that in the above equation $\hat{a}_{\rm in}^{(1)}$ is to be taken as the out-of-loop input field, i.e., $a_{\rm in}^{(1)}(t) = \varepsilon_s e^{-i\omega_s t}$.

Working in the frequency domain via the Fourier transform (for $o = a,\ m$)

$$\hat{o}(t) = \int d\omega \hat{o}[\omega]e^{-i\omega t}, \quad \text{(A18)}$$

we can solve the linear Heisenberg-Langevin equation for the coherent part of the fields, which gives us the relation between inputs and outputs

$$a_{\rm out}^{(i)}[\omega] = \sum_{j=1}^{2} S_{ij}[\omega]a_{\rm in}^{(j)}[\omega], \quad \text{(A19)}$$

where S is the scattering matrix of the system. Since only port 1 is coherently driven $a_{\rm in}^{(2)}[\omega_s] = 0$ and $a_{\rm in}^{(1)}[\omega] = \varepsilon_s\delta[\omega - \omega_s]$. Therefore $a_{\rm out}^{(2)}[\omega] = S_{21}[\omega]a_{\rm in}^{(1)}[\omega] = S_{21}[\omega]\varepsilon_s\delta[\omega - \omega_s]$. The transmission amplitude of a coherent tone with frequency ω_s is thus $S_{21}[\omega_s]$, as given in Eq. (5).

5. Magnomechanical interaction and polariton-phonon coupling

The magnon excitation inside the YIG sphere induces a time-dependent magnetization, which in turn deforms the sphere through magnetostrictive forces. Conversely, mechanical vibrations modify the magnetization, resulting in an intrinsic coupling between magnon and phonon modes [15,16]. Owing to the large frequency mismatch between magnons (GHz) and phonons (MHz), this interaction is naturally weak. To compensate for this mismatch and enhance the effective interaction, a strong coherent microwave drive is applied.

The magnetostrictive interaction is described by a radiation-pressure-like dispersive Hamiltonian [15],

$$\hat{H}_{mb}/\hbar = g_{mb}\hat{m}^\dagger\hat{m}(\hat{b} + \hat{b}^\dagger), \quad \text{(A20)}$$

where g_{mb} is the intrinsic magnomechanical coupling strength and $\hat{b}$ is the annihilation operator of the mechanical mode with resonance frequency ω_b. The single-magnon magnomechanical coupling g_{mb} depends on the sphere size and on magneto-elastic coefficients that are material-specific parameters [79,81].

Working in a frame rotating at the drive frequency ω_d, the linearized Hamiltonian of the driven cavity magnomechanical system, expressed in terms of the hybrid polariton modes, is given by

$$\frac{\hat{H}}{\hbar} = (\tilde{\omega}_+ - \omega_d)\hat{A}_+^\dagger\hat{A}_+ + (\tilde{\omega}_- - \omega_d)\hat{A}_-^\dagger\hat{A}_- + \omega_b\hat{b}^\dagger\hat{b} + (G_+\hat{A}_+^\dagger + G_+^*\hat{A}_+)(\hat{b} + \hat{b}^\dagger) + (G_-\hat{A}_-^\dagger + G_-^*\hat{A}_-)(\hat{b} + \hat{b}^\dagger) + \sqrt{2\kappa_{+,\mathrm{ext}}^{(1)}}\varepsilon_s(\hat{A}_+e^{i(\omega_s-\omega_d)t} + \hat{A}_+^\dagger e^{-i(\omega_s-\omega_d)t}) + \sqrt{2\kappa_{-,\mathrm{ext}}^{(1)}}\varepsilon_s(\hat{A}_-e^{i(\omega_s-\omega_d)t} + \hat{A}_-^\dagger e^{-i(\omega_s-\omega_d)t}), \quad \text{(A21)}$$

where

$$G_+ = g_{mb}(\sin^2\psi\tilde{A}_{+,\mathrm{ss}} + \sin\psi\cos\psi\tilde{A}_{-,\mathrm{ss}}), \quad \text{(A22)}$$

$$G_- = g_{mb}(\cos^2\psi\tilde{A}_{-,\mathrm{ss}} + \sin\psi\cos\psi\tilde{A}_{+,\mathrm{ss}}), \quad \text{(A23)}$$

and the steady state excitation in the simple single mode regime is

$$\tilde{A}_{\pm,\mathrm{ss}} = \frac{\sqrt{2\tilde{\kappa}_{\pm,\mathrm{ext}}^{(1)}}\varepsilon_d}{\tilde{\kappa}_\pm + i(\tilde{\omega}_\pm - \omega_d)}, \quad \text{(A24)}$$

$$\tilde{\kappa}_{\pm,\mathrm{ext}}^{(1)} = \frac{1 \pm \cos 2\psi}{2}\kappa_{\mathrm{ext}}^{(1)}. \quad \text{(A25)}$$

The strong coupling regime of polariton-phonon interaction enabled by microwave feedback manifests experimentally through interference effects in the probe response, which is studied both with and without feedback in Sec. III.

The transmission amplitude of the system S_{21} is obtained using the same procedure outlined above. The frequency at which the transmission amplitude in Eq. (7) is written is the difference between the weak probe drive frequency and the strong pump tone, as the Hamiltonian (A21) is written in a frame rotating at the pump frequency ω_d.

APPENDIX B: ADDITIONAL EXPERIMENTAL INFORMATION

1. Measured and theoretical transmission spectra as a function of feedback gain

For completeness, Fig. 5 shows the same experimental and theoretical data presented in Fig. 2(c), displayed as two-dimensional color maps to provide a global view of the evolution of the transmission spectra with increasing feedback gain. The theoretical spectra are obtained from Eq. (7) using the fitting procedure described in Sec. III. The excellent agreement between experiment and theory over the entire feedback-gain range confirms that Eq. (7) accurately captures the feedback-modified polariton-phonon dynamics, including the evolution from magnomechanically induced transparency to normal-mode splitting.

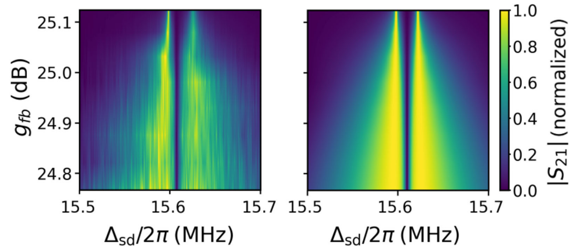

FIG. 5. Measured (left) and theoretical (right) transmission amplitude, $|S_{21}|$, of the upper cavity-magnon polariton as a function of the feedback gain g_{fb}. The theoretical spectra are obtained from Eq. (7) using the fitting procedure described in Sec. III. The comparison demonstrates excellent agreement over the entire feedback-gain range.

2. Experimental calibration of the feedback-loop efficiency

The feedback-loop efficiency η appearing in Eqs. (1) and (2) quantifies the effective coherent transmission from the cavity output to the feedback input. This parameter includes the cumulative effect of insertion losses from the phase shifter, directional couplers, microwave cables, connectors, and residual impedance mismatches in the feedback path.

Experimentally, η is extracted by comparing the measured transmission of the complete feedback path with the independently measured transmission of the amplifier chain. Specifically, we define

$$\eta(\omega, g_{\mathrm{fb}}) = \frac{|S_{21}^{\mathrm{loop}}(\omega, g_{\mathrm{fb}})|^2}{|S_{21}^{\mathrm{amp}}(\omega, g_{\mathrm{fb}})|^2}, \quad \text{(B1)}$$

where S_{21}^{loop} is the measured transmission of the complete feedback path and S_{21}^{amp} is the independently measured transmission of the amplifier chain.

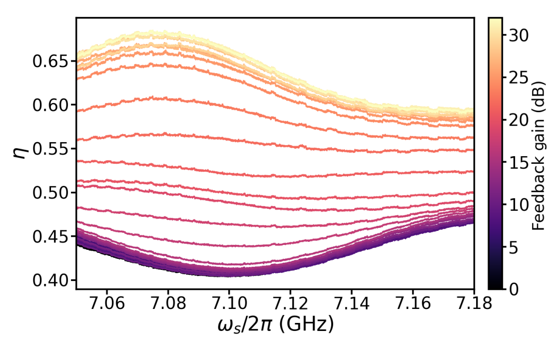

FIG. 6. Experimental calibration of the feedback-loop efficiency. The extracted efficiency $\eta(\omega_s, g_{\mathrm{fb}}) = |S_{21}^{\mathrm{loop}}(\omega_s, g_{\mathrm{fb}})|^2/|S_{21}^{\mathrm{amp}}(\omega_s, g_{\mathrm{fb}})|^2$ is plotted as a function of frequency for different feedback-gain settings. The efficiency accounts for insertion losses from the phase shifter, directional couplers, isolator, microwave cables, connectors, and residual impedance mismatches in the feedback path. In the gain range used for the feedback measurements, the extracted efficiency is approximately $\eta \simeq 0.6$.

The extracted efficiency is shown in Fig. 6. Over the frequency range relevant to the feedback measurements, η lies between approximately 0.4 and 0.65, depending weakly on frequency and feedback gain. In the gain range used for the main feedback measurements, the efficiency is approximately $\eta \simeq 0.6$, indicating that the feedback path introduces only moderate insertion losses while maintaining efficient microwave transmission over the operating frequency range. This level of efficiency is comparable to those achieved in feedback-based cavity optomechanical experiments [51,53], although the reported efficiencies refer to different experimental implementations. We therefore treat η as an effective experimental parameter describing the overall coherent transmission of the feedback path under the operating conditions of the experiment.

3. Physical meaning of negative effective cavity damping

The measurements present throughout the paper concern the hybrid cavity-magnon system, for which the physically relevant dissipation rates are the polariton linewidths, $\tilde{\kappa}_{\pm}$. An interesting question, however, is the physical interpretation of the effective cavity dissipation rate, $\tilde{\kappa}_a$, when Eq. (A11) predicts negative values. In particular, a negative $\tilde{\kappa}_a$ formally corresponds to a regime in which the feedback-induced gain exceeds the intrinsic cavity loss. To investigate the physical meaning of this regime and the validity of the linear model, we performed independent measurements of the bare cavity, which is used in the experiment, operated inside the same feedback loop.

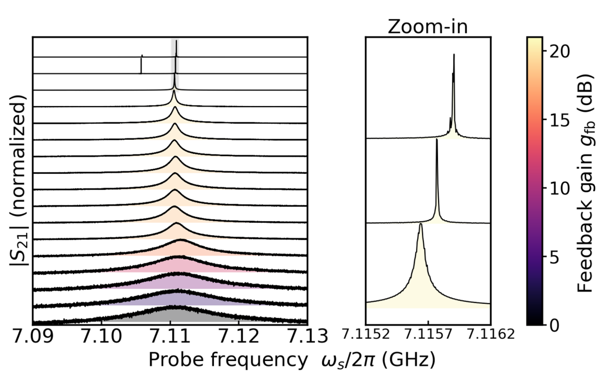

FIG. 7. Measured transmission spectrum of the bare cavity for different feedback gains. Increasing the feedback gain progressively narrows the cavity resonance, consistent with the reduction of the effective cavity damping rate predicted by the linear feedback model. The right panel presents an enlarged view of the spectra measured at the three highest feedback gains ($g_{\rm fb} = 20.50$, 20.75, and 21.00 dB), showing the pronounced linewidth narrowing at 20.50 dB and the onset of spectral distortion at 20.75 and 21.00 dB as the system approaches the instability threshold. Near the instability threshold, the cavity response becomes distorted and can no longer be described by a simple Lorentzian line shape.

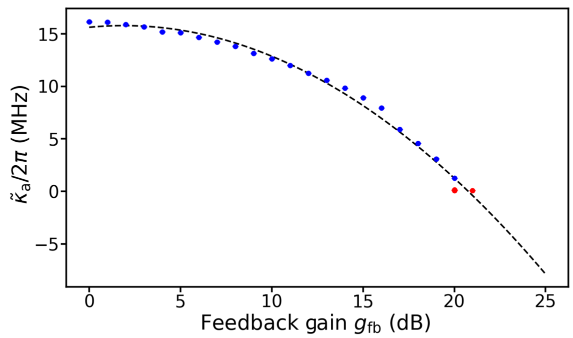

FIG. 8. Extracted bare-cavity linewidth as a function of the feedback gain. The dashed line shows the prediction of the linear feedback model, while the symbols represent the experimental data. The blue symbols correspond to the stable operating regime, where the measured linewidth is in good agreement with the linear theory. The red symbols denote measurements performed beyond the stability threshold. In this regime, the bare-cavity spectrum becomes distorted due to the onset of instability, preventing a reliable Lorentzian description. Consequently, the extracted linewidth no longer follows the prediction of the linear feedback model, indicating the breakdown of the linear steady-state approximation.

Figure 7 shows the measured transmission spectrum of the bare cavity for different feedback gains. As expected from Eq. (A11), increasing the feedback gain progressively reduces the cavity linewidth. However, as the gain approaches the value for which the linear theory predicts $\tilde{\kappa}_a \to 0$, the cavity response becomes increasingly distorted and can no longer be described by a simple Lorentzian spectrum.

Figure 8 compares the experimentally extracted cavity linewidth with the prediction of Eq. (A11). Good agreement is observed at moderate feedback gains. Near the instability threshold, however, the measured linewidth deviates from the linear prediction and remains finite, indicating the breakdown of the linear steady-state description.

[1] G. Kurizki, P. Bertet, Y. Kubo, K. Mølmer, D. Petrosyan, P. Rabl, and J. Schmiedmayer, *Quantum technologies with hybrid systems*, Proc. Natl. Acad. Sci. U.S.A. **112**, 3866 (2015).
[2] T. Trickle, Z. Zhang, and K. M. Zurek, *Detecting light dark matter with magnons*, Phys. Rev. Lett. **124**, 201801 (2020).
[3] C. Chang, T. J. Hobbs, D. Jin, Y. Li, M. Lisovenko, V. Novosad, Z. H. Saleem, T. Trickle, and G. Wang, *Searching for axion dark matter with array-scalable single magnon detectors*, Phys. Rev. D **113**, 015016 (2026).
[4] Y. Li, J. C. Qian, Z. H. Jiang, T. H. Lo, D. Ding, T. Draher, T. Polakovic, W. Pfaff, A. Schleife, J. M. Zuo, W. K. Kwok, V. Novosad, and A. Hoffmann, *Hybrid-magnon quantum devices: Strategies and approaches*, in *Technical Digest—International Electron Devices Meeting, IEDM* (Institute of Electrical and Electronics Engineers (IEEE), San Francisco, CA, USA, 2022), Vol. 2022.

[5] M. Kim, A. Tabesh, T. Zegray, S. Barzanjeh, and C. M. Hu, *Nonreciprocity in cavity magnonics at millikelvin temperature*, J. Appl. Phys. **135**, 063904 (2024).
[6] J. Jia, Y. Li, J. Huang, and M. Zhang, *Nonreciprocal quantum coherence in a cavity magnomechanical system via the barnett effect*, Phys. Rev. A **113**, 013719 (2026).
[7] F. Engelhardt, V. A. S. V. Bittencourt, H. Huebl, O. Klein, and S. V. Kusminskiy, *Optimal broadband frequency conversion via a magnetomechanical transducer*, Phys. Rev. Appl. **18**, 044059 (2022).
[8] Ö. O. Soykal and M. E. Flatté, *Strong field interactions between a nanomagnet and a photonic cavity*, Phys. Rev. Lett. **104**, 077202 (2010).
[9] H. Huebl, C. W. Zollitsch, J. Lotze, F. Hocke, M. Greifenstein, A. Marx, R. Gross, and Sebastian T. Goennenwein, *High cooperativity in coupled microwave resonator ferrimagnetic insulator hybrids*, Phys. Rev. Lett. **111**, 127003 (2013).
[10] Y. Tabuchi, S. Ishino, T. Ishikawa, R. Yamazaki, K. Usami, and Y. Nakamura, *Hybridizing ferromagnetic magnons and microwave photons in the quantum limit*, Phys. Rev. Lett. **113**, 083603 (2014).
[11] M. Goryachev, W. G. Farr, D. L. Creedon, Y. Fan, M. Kostylev, and M. E. Tobar, *High-cooperativity cavity QED with magnons at microwave frequencies*, Phys. Rev. Appl. **2**, 054002 (2014).
[12] C. A. Potts and J. P. Davis, *Strong magnon-photon coupling within a tunable cryogenic microwave cavity*, Appl. Phys. Lett. **116**, 263503 (2020).
[13] M. S. Ebrahimi, A. Motazedifard, and M. B. Harouni, *Single-quadrature quantum magnetometry in cavity electromagnonics*, Phys. Rev. A **103**, 062605 (2021).
[14] M. S. Ebrahimi and M. B. Harouni, *Parity-time symmetry-enhanced simultaneous magnon and photon blockade in cavity magnonic system*, J. Phys. B **56**, 235501 (2023).
[15] X. Zhang, C. L. Zou, L. Jiang, and H. X. Tang, *Cavity magnomechanics*, Sci. Adv. **2**, e1501286 (2016).
[16] C. A. Potts, E. Varga, V. A. S. V. Bittencourt, S. V. Kusminskiy, and J. P. Davis, *Dynamical backaction magnomechanics*, Phys. Rev. X **11**, 031053 (2021).
[17] J. Li, S. Y. Zhu, and G. S. Agarwal, *Magnon-photon-phonon entanglement in cavity magnomechanics*, Phys. Rev. Lett. **121**, 203601 (2018).
[18] J. Li and S. Y. Zhu, *Entangling two magnon modes via magnetostrictive interaction*, New J. Phys. **21**, 085001 (2019).
[19] J. M. Nair and G. S. Agarwal, *Deterministic quantum entanglement between macroscopic ferrite samples*, Appl. Phys. Lett. **117**, 084001 (2020).
[20] J. Li and S. Groblacher, *Entangling the vibrational modes of two massive ferromagnetic spheres using cavity magnomechanics*, Quantum Sci. Technol. **6**, 024005 (2021).
[21] M. S. Ding, X. X. Xin, S. Y. Qin, and C. Li, *Enhanced entanglement and steering in pt -symmetric cavity magnomechanics*, Opt. Commun. **490**, 126903 (2021).
[22] H.-J. Cheng, S.-J. Zhou, J.-X. Peng, A. Kundu, H.-X. Li, L. Jin, and X.-L. Feng, *Tripartite entanglement in a Laguerre-Gaussian rotational-cavity system with an yttrium iron garnet sphere*, J. Opt. Soc. Am. B **38**, 285 (2021).
[23] J. Li, S. Y. Zhu, and G. S. Agarwal, *Squeezed states of magnons and phonons in cavity magnomechanics*, Phys. Rev. A **99**, 021801(R) (2019).
[24] X. Li, W.-X. Yang, T. Shui, L. Li, X. Wang, and Z. Wu, *Phase control of the transmission in cavity magnomechanical system with magnon driving*, J. Appl. Phys. **128**, 233101 (2020).
[25] B. Sarma, T. Busch, and J. Twamley, *Cavity magnomechanical storage and retrieval of quantum states*, New J. Phys. **23**, 043041 (2021).
[26] J. Zhao, L. Wu, T. Li, Y. X. Liu, F. Nori, Y. Liu, and J. Du, *Phase-controlled pathway interferences and switchable fast-slow light in a cavity-magnon polariton system*, Phys. Rev. Appl. **15**, 024056 (2021).
[27] C. A. Potts, V. A. S. V. Bittencourt, S. V. Kusminskiy, S. V. Kusminskiy, and J. P. Davis, *Magnon-phonon quantum correlation thermometry*, Phys. Rev. Appl. **13**, 064001 (2020).
[28] V. A. Bittencourt, C. A. Potts, J. P. Davis, and A. Metelmann, *Magnon-microwave backaction noise evasion in cavity magnomechanics*, Commun. Phys. **8**, 247 (2025).
[29] M. Wang, D. Zhang, X. H. Li, Y. Y. Wu, and Z. Y. Sun, *Magnon chaos in pt-symmetric cavity magnomechanics*, IEEE Photonics J. **11** (2019).
[30] A. Suleymanzade, A. Anferov, M. Stone, R. K. Naik, A. Oriani, J. Simon, and D. Schuster, *A tunable high-q millimeter wave cavity for hybrid circuit and cavity QED experiments*, Appl. Phys. Lett. **116**, 104001 (2020).
[31] M. Kudra, J. Biznárová, A. F. Roudsari, J. J. Burnett, D. Niepce, S. Gasparinetti, B. Wickman, and P. Delsing, *High quality three-dimensional aluminum microwave cavities*, Appl. Phys. Lett. **117**, 070601 (2020).
[32] L. Shi, T. Guo, R. Su, T. Chi, Y. Sheng, J. Jiang, C. Cao, J. Wu, X. Tu, G. Sun, J. Chen, and P. Wu, *Tantalum microwave resonators with ultra-high intrinsic quality factors*, Appl. Phys. Lett. **121**, 242601 (2022).
[33] Y. Cao and P. Yan, *Exceptional magnetic sensitivity of pt-symmetric cavity magnon polaritons*, Phys. Rev. B **99**, 214415 (2019).
[34] J. W. Rao, Y. P. Wang, Y. Yang, T. Yu, Y. S. Gui, X. L. Fan, D. S. Xue, and C. M. Hu, *Interactions between a magnon mode and a cavity photon mode mediated by traveling photons*, Phys. Rev. B **101**, 064404 (2020).
[35] M. Harder, B. M. Yao, Y. S. Gui, and C. M. Hu, *Coherent and dissipative cavity magnonics*, J. Appl. Phys. **129**, 201101 (2021).
[36] B. Z. Rameshti, S. V. Kusminskiy, J. A. Haigh, K. Usami, D. Lachance-Quirion, Y. Nakamura, C. M. Hu, H. X. Tang, G. E. Bauer, and Y. M. Blanter, *Cavity magnonics*, Phys. Rep. **979**, 1 (2022).
[37] A. Gardin, J. Bourhill, V. Vlaminck, C. Person, C. Fumeaux, V. Castel, and G. C. Tettamanzi, *Manifestation of the coupling phase in microwave cavity magnonics*, Phys. Rev. Appl. **19**, 054069 (2023).
[38] X. Zhang, C. L. Zou, L. Jiang, and H. X. Tang, *Strongly coupled magnons and cavity microwave photons*, Phys. Rev. Lett. **113**, 156401 (2014).
[39] T. Wolz, A. Stehli, A. Schneider, I. Boventer, R. Macêdo, A. V. Ustinov, M. Kläui, and M. Weides, *Introducing coherent time control to cavity magnon-polariton modes*, Commun. Phys. **3**, 3 (2020).

[40] J. Xu, C. Zhong, X. Han, D. Jin, L. Jiang, and X. Zhang, *Floquet cavity electromagnonics*, Phys. Rev. Lett. **125**, 237201 (2020).

[41] J. Xu, C. Zhong, X. Han, D. Jin, L. Jiang, and X. Zhang, *Coherent gate operations in hybrid magnonics*, Phys. Rev. Lett. **126**, 207202 (2021).

[42] Y. Li, V. G. Yefremenko, M. Lisovenko, C. Trevillian, T. Polakovic, T. W. Cecil, P. S. Barry, J. Pearson, R. Divan, V. Tyberkevych, C. L. Chang, U. Welp, W. K. Kwok, and V. Novosad, *Coherent coupling of two remote magnonic resonators mediated by superconducting circuits*, Phys. Rev. Lett. **128**, 047701 (2022).

[43] A. Girich, S. Nedukh, S. Polevoy, K. Sova, S. Tarapov, and A. Vakula, *Enhancement of the microwave photon-magnon coupling strength for a planar fabricated resonator*, Sci. Rep. **13**, 924 (2023).

[44] B. Yao, Y. S. Gui, J. W. Rao, Y. H. Zhang, W. Lu, and C. M. Hu, *Coherent microwave emission of gain-driven polaritons*, Phys. Rev. Lett. **130**, 146702 (2023).

[45] J. Yao, C. Lu, X. Fan, D. Xue, G. E. Bridges, and C. M. Hu, *Nonreciprocal control of the speed of light using cavity magnonics*, Phys. Rev. Lett. **134**, 196904 (2025).

[46] M. Song, T. Polakovic, J. Lim, T. W. Cecil, J. Pearson, R. Divan, W. K. Kwok, U. Welp, A. Hoffmann, K. J. Kim, V. Novosad, and Y. Li, *Single-shot magnon interference in a magnon-superconducting-resonator hybrid circuit*, Nat. Commun. **16**, 3649 (2025).

[47] Z. Q. Wang, Z. Y. Wang, Y. P. Wang, and J. Q. You, *Single-mode magnon-polariton lasing and amplification controlled by dissipative coupling*, Phys. Rev. Lett. **135**, 186704 (2025).

[48] N. J. Lambert, A. Schumer, J. J. Longdell, S. Rotter, and H. G. Schwefel, *Coherent control of magnon-polaritons using an exceptional point*, Nat. Phys. **21**, 1570 (2025).

[49] Y. S. Gui and C.-M. Hu, *Gain-driven polaritons for high-sensitivity wireless magnetic sensing*, APL Quantum **3**, 026110 (2026).

[50] M. Ebrahimi, Y. Huang, A. Rashedi, and J. P. Davis, *Coherent perfect absorption: Zero reflection without linewidth suppression*, arXiv:2510.22358.

[51] M. Rossi, N. Kralj, S. Zippilli, R. Natali, A. Borrielli, G. Pandraud, E. Serra, G. Di Giuseppe, and D. Vitali, *Enhancing sideband cooling by feedback-controlled light*, Phys. Rev. Lett. **119**, 123603 (2017).

[52] M. Rossi, N. Kralj, S. Zippilli, R. Natali, A. Borrielli, G. Pandraud, E. Serra, G. Di Giuseppe, and D. Vitali, *Normal-mode splitting in a weakly coupled optomechanical system*, Phys. Rev. Lett. **120**, 073601 (2018).

[53] M. Rossi, D. Mason, J. Chen, Y. Tsaturyan, and A. Schliesser, *Measurement-based quantum control of mechanical motion*, Nature (London) **563**, 53 (2018).

[54] S. Zippilli, N. Kralj, M. Rossi, G. Di Giuseppe, and D. Vitali, *Cavity optomechanics with feedback-controlled in-loop light*, Phys. Rev. A **98**, 023828 (2018).

[55] G. Serafini, S. Zippilli, and I. Marzoli, *Optomechanical stirling heat engine driven by feedback-controlled light*, Phys. Rev. A **102**, 053502 (2020).

[56] M. S. Ebrahimi, S. Zippilli, and D. Vitali, *Feedback-enabled microwave quantum illumination*, Quantum Sci. Technol. **7**, 035003 (2022).

[57] C. Wang, L. Banniard, L. M. de Lépinay, and M. A. Sillanpää, *Fast feedback control of mechanical motion using circuit optomechanics*, Phys. Rev. Appl. **19**, 054091 (2023).

[58] M. Ernzer, M. Bosch Aguilera, M. Brunelli, G. L. Schmid, T. M. Karg, C. Bruder, P. P. Potts, and P. Treutlein, *Optical coherent feedback control of a mechanical oscillator*, Phys. Rev. X **13**, 021023 (2023).

[59] L. Du, J. Monsel, W. Wieczorek, and J. Splettstoesser, *Coherent feedback control for cavity optomechanical systems with a frequency-dependent mirror*, Phys. Rev. A **111**, 013506 (2025).

[60] E. Rej, R. Cutting, J. Depellette, D. Datta, N. Tiencken, J. Govenius, V. Vesterinen, Y. Liu, and M. A. Sillanpää, *Near-ground-state cooling in electromechanics using measurement-based feedback and a Josephson traveling-wave parametric amplifier*, Phys. Rev. Appl. **23**, 034009 (2025).

[61] S. Gröblacher, K. Hammerer, M. R. Vanner, and M. Aspelmeyer, *Observation of strong coupling between a micromechanical resonator and an optical cavity field*, Nature (London) **460**, 724 (2009).

[62] J. D. Teufel, D. Li, M. S. Allman, K. Cicak, A. J. Sirois, J. D. Whittaker, and R. W. Simmonds, *Circuit cavity electromechanics in the strong-coupling regime*, Nature (London) **471**, 204 (2011).

[63] A. Schliesser, R. Rivière, G. Anetsberger, O. Arcizet, and T. J. Kippenberg, *Resolved-sideband cooling of a micromechanical oscillator*, Nat. Phys. **4**, 415 (2008).

[64] J. D. Teufel, T. Donner, D. Li, J. W. Harlow, M. S. Allman, K. Cicak, A. J. Sirois, J. D. Whittaker, K. W. Lehnert, and R. W. Simmonds, *Sideband cooling of micromechanical motion to the quantum ground state*, Nature (London) **475**, 359 (2011).

[65] J. Chan, T. P. Alegre, A. H. Safavi-Naeini, J. T. Hill, A. Krause, S. Gröblacher, M. Aspelmeyer, and O. Painter, *Laser cooling of a nanomechanical oscillator into its quantum ground state*, Nature (London) **478**, 89 (2011).

[66] T. X. Lu, H. Zhang, Q. Zhang, and H. Jing, *Exceptional-point-engineered cavity magnomechanics*, Phys. Rev. A **103**, 063708 (2021).

[67] S. Chakraborty and C. Das, *Nonreciprocal magnon-photon-phonon entanglement in cavity magnomechanics*, Phys. Rev. A **108**, 063704 (2023).

[68] M. Amazioug, B. Teklu, and M. Asjad, *Enhancement of magnon-photon-phonon entanglement in a cavity magnomechanics with coherent feedback loop*, Sci. Rep. **13**, 3833 (2023).

[69] H. Qian, X. Zuo, Z. Y. Fan, J. Cheng, and J. Li, *Strong squeezing of microwave output fields via reservoir-engineered cavity magnomechanics*, Phys. Rev. A **109**, 013704 (2024).

[70] T. X. Lu, Z. S. Li, L. S. Chen, Y. Wang, X. Xiao, and H. Jing, *Nonreciprocal entanglement in cavity magnomechanics via the Barnett effect*, Phys. Rev. A **111**, 013713 (2025).

[71] Y. Tabuchi, S. Ishino, A. Noguchi, T. Ishikawa, R. Yamazaki, K. Usami, and Y. Nakamura, *Coherent coupling between a ferromagnetic magnon and a superconducting qubit*, Science **349**, 405 (2015).

[72] S. Weis, R. Rivière, S. Deléglise, E. Gavartin, O. Arcizet, A. Schliesser, and T. J. Kippenberg, *Optomechanically induced transparency*, Science **330**, 1520 (2010).

[73] I. Mahboob, K. Nishiguchi, H. Okamoto, and H. Yamaguchi, *Phonon-cavity electromechanics*, Nat. Phys. **8**, 387 (2012).

[74] M. Aspelmeyer, T. J. Kippenberg, and F. Marquardt, *Cavity optomechanics*, Rev. Mod. Phys. **86**, 1391 (2014).

[75] C. Galland, N. Sangouard, N. Piro, N. Gisin, and T. J. Kippenberg, *Heralded single-phonon preparation, storage, and readout in cavity optomechanics*, Phys. Rev. Lett. **112**, 143602 (2014).

[76] A. A. Rakhubovsky and R. Filip, *Photon-phonon-photon transfer in optomechanics*, Sci. Rep. **7**, 46764 (2017).

[77] H. K. Lau and A. A. Clerk, *Ground-state cooling and high-fidelity quantum transduction via parametrically driven bad-cavity optomechanics*, Phys. Rev. Lett. **124**, 103602 (2020).

[78] C. Schäfermeier, H. Kerdoncuff, U. B. Hoff, H. Fu, A. Huck, J. Bilek, G. I. Harris, W. P. Bowen, T. Gehring, and U. L. Andersen, *Quantum enhanced feedback cooling of a mechanical oscillator using nonclassical light*, Nat. Commun. **7**, 13628 (2016).

[79] V. A. S. V. Bittencourt, C. A. Potts, Y. Huang, J. P. Davis, and S. V. Kusminskiy, *Magnomechanical backaction corrections due to coupling to higher-order walker modes and kerr nonlinearities*, Phys. Rev. B **107**, 144411 (2023).

[80] A. A. Clerk, M. H. Devoret, S. M. Girvin, F. Marquardt, and R. J. Schoelkopf, *Introduction to quantum noise, measurement, and amplification*, Rev. Mod. Phys. **82**, 1155 (2010).

[81] C. Gonzalez-Ballestero, D. Hümmer, J. Gieseler, and O. Romero-Isart, *Theory of quantum acoustomagnonics and acoustomechanics with a micromagnet*, Phys. Rev. B **101**, 125404 (2020).